P3.31

ESTIMATING THE REPRESENTATION OF EXTREME PRECIPITATION EVENTS IN ATMOSPHERIC GENERAL CIRCULATION MODELS USING *L*-MOMENTS

L. Marx*
Center for Ocean-Land-Atmosphere Studies (COLA), Calverton, MD

1. INTRODUCTION

Climate simulation and prediction, even when using physically based models, gives rise to a non-deterministic perspective of the manifold states of the Earth's climate. This requires making estimations through multiple realizations spanning the entire annual cycle through many years and locations. Ensemble averaging in this situation, unlike that in weather prediction, can lead to an underestimation of the climate variability and extreme behavior. Yet it is often the more extreme states that are of interest to the public and that provide the greatest potential benefit by foreseeing their onset. This can be achieved by estimating both the observed and model probability distributions establishing whether the model can represent observed extreme values and determining whether a shift in the model ensemble distribution suggests a likely threat of an extreme event.

For nearly every location throughout the world, particularly in inhabited ones, precipitation is an important climate variable. While at some locations precipitation is nearly normally distributed on an annual mean basis, as averaging periods become shorter, distributions are almost always non-normal. At many other locations precipitation remains non-normally distributed even after several years and may require several decades before central limit theorem conditions become realized. As the distribution becomes different from normal, the use of normally based statistical methods will converge more slowly and may never reach any usable level of significance even with large ensembles. Estimating distributions of observed precipitation are further limited by having only one realization.

Two methods employed more frequently to estimate distribution are Maximum Likelihood Estimators (MLEs) and Bayesian estimators. MLEs still require a larger sample size (>100) than is often available and Bayesian estimators work best when the underlying distribution is close to the *a priori* distribution. Otherwise the convergence rate will probably not exceed that of MLEs. The newer method of *L*-moment estimators (Hosking and Wallis, 1997, referred hereafter as HW), makes it possible to obtain reasonable estimates for sample sizes as small as 20 without any assumed distribution.

In this study two atmospheric general circulation models (AGCMs) will be studied: COLA V2.2.6 and NASA Goddard Space Flight Center (GSFC) Seasonal-to-Interannuall Prediction Project (NSIPP) and compared with gridded Climate Anomaly Monitoring Station (Ropelewski et al., 1985) data for two regions in two separate months: Europe (30°N-70°N, 10°W-40°E) in December and South Asia (5°N-35°N, 70°E-125°E) in July. These were selected to give an idea of seasonal precipitation behavior in a month where the seasonal activity is well represented throughout the region. The distribution of two higher *L*-moments (τ_3 and τ_4) as an indication of the distribution function distribution will be presented.

2. ANALYSIS METHOD

2.1 *L-moments*

L-moments are described briefly in von Storch and Zwiers (1999) and in more detail in HW. Using the uniform distribution function as its foundation and based on shifted Legendre polynomials, each statistical *L*-moment is computed linearly (hence the *L*) giving a more robust estimate for a given amount of data than other methods. This method relies on sorting (ordering) the data by value. If the i'th rank value in a sorted sample vector of length n is denoted by $X_{i:n}$ and E is the expected value function, then the first four *L*-moments are given by:

$$\lambda_1 = E(X_{1:1})$$
$$\lambda_2 = \tfrac{1}{2}E(X_{2:2} - X_{1:2})$$
$$\lambda_3 = \tfrac{1}{3}E(X_{3:3} - 2X_{2:3} + X_{1:3})$$
$$\lambda_4 = \tfrac{1}{4}E(X_{4:4} - X_{3:4} + X_{2:4} - X_{1:4})$$

The estimates of these can be computed in a straightforward manner using combinatorics found in the above references.

The second moment is often scaled by the

* *Corresponding author address*: L. Marx, Center for Ocean-Land-Atmosphere Studies, 4041 Powder Mill Road, Suite 302, Calverton, MD 20705; e-mail: marx@cola.iges.org

mean so that a coefficient of variability is determined:

L-CV=$\tau=\lambda_2/\lambda_1$

Higher moments are usually scaled by the second moment giving:

$\tau_3=\lambda_3/\lambda_2$

and

$\tau_4=\lambda_4/\lambda_2$

Unlike standard moments, τ_3 and τ_4 are constrained to be between −1 and +1 and further τ_4 is constrained by τ_3 to be no lower that −0.25. Because precipitation is non-negative, τ is also constrained to range from 0 to 1.

2.2 *Modified Index-Flood Procedure*

The index-flood procedure detailed in HW was designed for multiple stations or sites within a sample region. The procedure presented here is modified for use with gridded data. With gridded data there is a possibility of some points having a heterogenous distribution that in the original procedure would be treated by shifting the sample region boundaries. As the heterogeneities cannot be entirely removed from the gridded data, less emphasis will be placed on achieving homogenous distribution estimates. Since the details of the procedure steps are quite lengthy, only the changes to the procedure will be given.

In this procedure the sample region is replaced with a moving overlay. The overlay consists of 9 grid points or boxes with a center point and its 8 surrounding points. Up to all 8 surrounding points are included with the center point providing a better estimate of the higher L-moments (>1) of the center point than single point (called "at site" in HW) calculations. The center point mean remains unchanged, thus retaining some of the individual character of the center point. While points at further distance could also be used, given the typical spatial distances in the models and analysis used here and the greater likelihood of decorrelation, including them seemed harder to justify and would further complicate this procedure.

As in HW, precipitation at each point is viewed as a mixed distribution with exact zero values excluded from analysis, but the probability of zero estimated from the sample so that it is included as part of the cumulative distribution estimate. From these data two screenings are done: discordancy and heterogeneity.

2.2.1 *Discordancy*

Discordancy, D, is based on a matrix of values for each point using τ, τ_3, and τ_4 as a 3-dimensional vector. This was intended to screen for suspect measurement data within the sample region. In this procedure no model data is considered suspect in this regard and any observed gridded data is assumed to have already be screened for bad values. This measure is retained, but the center point is never allowed to be rejected as being too discordant. Instead a new simpler measure is introduced, relative discordancy=D_R, which is the vector distance between the (τ, τ_3, τ_4) of the center point and each of the 8 surrounding points. The surrounding point with highest D_R is rejected and removed from further calculations involving the center point whenever D becomes too large. D and D_R are then recalculated based on the remaining points.

2.2.2 *Heterogeneity*

From each of the remaining points, the L-moments are calculated and average weighted by the non-zero lengths to form a "regional" or overlay average for the center point. Heterogeneity, H, is calculated as in HW based on a Monte Carlo simulation of data having the same L-moments as the center point overlay average but with mean 1. H is computed in three ways based on combinations of the dispersion (mean squared difference) of the simulated τ, τ_3, and τ_4 about their mean with appropriate scaling factors. When any of the three H values becomes too large, the maximum D_R point is rejected as above and recalculation is also done.

No more than 4 rejections are permitted. This prevents the matrix to compute D from becoming singular and assures a robust if heterogeneous distribution estimate. The 5 remaining points are used however large D and H remain, but the point is noted for further review. At this point in the procedure the estimation of the L-moments for the center point is finished and the selection of a suitable distribution function is done as in HW.

3. ANALYZED DATA

The Climate Anomaly Monitoring Station (CAMS) precipitation data has been interpolated to an R40 Gaussian grid (128x102) using an objective analysis scheme (Doty, private communication). The data extends back several decades, but only a more recent period of 55 years (1948-2002) has been used. This data is primarily over land only with some islands included. For comparison the model data will be similarly focused.

The V2.2.6 COLA AGCM, a slight modification of the model described in Schneider (2002) was used in the Climate of the Twentieth Century (C20C) (Folland and Kinter, 2002) experiment with the 10 ensemble member results saved from December 1948 through November

2002.

The NSIPP 1 (Pegion, et al., 2000) model was also used in the C20C experiment with 14 ensemble members, while starting in January 1902, also covered the same period as COLA V2.2.6.

Both model results were interpolated to the R40 grid of CAMS.

4. RESULTS

Figures 1, 2 and 3 show the scatter plot distribution of t_3 and t_4 (the estimates of τ_3 and τ_4) at each point for CAMS, COLA and GSFC (NSIPP) respectively for Europe in December. For the models each ensemble member is shown in a different color. For the NSIPP model only 10 of the 14 ensemble members are shown to aid comparison. In addition locations of some two-parameter distributions are shown with large filled circles and three-parameter distributions are drawn as curves. The two-parameter distributions are:

Color	Letter	Distribution
Yellow	L	Logistic
Orange	U	Uniform
Black	G	Gumbel
Blue	N	Normal
Purple	E	Exponential

The three-parameter distributions are:

Color	Letters	Distribution
Green	OLB	Overall Lower Bound of all distributions
Yellow	GLO	Generalized Logistic
Orange	GPA	Generalized Pareto
Black	GEV	Generalized Extreme Value
Blue	GNO	Generalized Normal
Purple	PE3	Pearson type III (Gamma)

Details on the properties and formulas for these and other distributions can be found in Reiss and Thomas (2000).

The CAMS values are clustered near the GEV, GNO and PE3 curves with a centroid slightly less *L*-skewed than the Gumbel distribution. Few points are close to the normal distribution, only 3 points show negative *L*-skewness and no points are near the uniform distribution. Most points fall below the general logistic distribution, above the generalized Pareto distribution and have less *L*-skewness than the exponential distribution. Those that have higher *L*-skewness, tend to follow one of the above distributions. Points with large positive skewness indicate a distribution with a few very large values.

It can be seen that COLA does not come close to the CAMS centroid of the distribution and tends to have substantial negative skewness at several locations suggesting that the model seldom attains large values since precipitation itself is never negative. It also has many points near normal. Values can also get close to the uniform distribution. Some values become very positively skewed and don't align as much with the above distributions. The clustering overall is not as tight as CAMS and can reach unusual values more often, such as the generalized Pareto distribution when the *L*-skewness is small. All these problems suggest difficulty in representing the European rainfall realistically in the model.

The NSIPP has fewer negative skewness points but can have large positive skewness values like COLA and also gets closer to the uniform distribution (the origin) than CAMS. It is more tightly clustered and has its centroid closer to that of CAMS. It thus seems to have fewer problems than the COLA model.

Figures 4, 5 and 6 show the scatter plot distribution of t_3 and t_4 at each point for CAMS, COLA and GSFC (NSIPP) respectively for South Asia in July. The two- and three-parameter distributions are shown as in figures 1, 2 and 3. Some model points were excluded due to fewer than 15 non-zero values or low mean (<0.125 mm/day) values. The CAMS data had no such points.

Here the CAMS points are less tightly clustered but have close to the same centroid as Europe. More negative *L*-skewness values are seen, and larger positive values are reached as well. The uniform distribution is generally avoided, and there are few points near normal. However the generalized logistic is often exceeded above and generalized Pareto is sometimes exceeded below. There still seems some preference for following near the curves at higher *L*-skewness.

The COLA model is closer to CAMS for South Asia than for Europe but still has disproportionately too many negatively skewed points and is not quite as tightly clustered. While the generalized logistic and generalized Pareto curves seem to be even less of a barrier, there is a

generally matching spread of the points as *L*-skewness increases.

The NSIPP model has more problems in this region with far more negative *L*-skewness values and fewer large positive values. The clustering is far tighter than CAMS and suggests too little variability in comparison to the CAMS distribution. Here representing realistic rainfall is more of a problem.

5. CONCLUSIONS

This method of employing *L*-moments to estimate the distribution of model precipitation and comparing the model's ability to realistically represent extreme values seems promising as yet another evaluation tool. Certain areas, such as deserts, where too little precipitation falls or is too infrequent are unsuitable for this method. However, many areas will have enough usable data to obtain an estimate of their behavior, and these are likely to have many people with a need for realistic predictions.

6. REFERENCES

Folland, C. and J. L. Kinter III, 2002: The Climate of the Twentieth Century Project. *CLIVAR Exchanges*, **7(2)**, 37-39.

Hosking, J. R. M. and J. R. Wallis, 1997: *Regional Frequency Analysis*. Cambridge University Press.

Pegion, P. J., S. D. Schubert, and M. J. Suarez, 2000: An Assessment of the Predictability of Northern Winter Seasonal Means with the NSIPP 1 AGCM, NASA/TM-2000-104606, Vol. 18.

Reiss, R.-D. and M. Thomas, 2000: *Statistical Analysis of Extreme Values*. Birkhäuser Verlag, Basel.

Ropelewski, C. F., J. E. Janowiak and M. F. Halpert, 1985: The analysis and display of real time surface climate data. *Mon. Wea. Rev.*, **113**, 1101-1107.

Schneider, E. K., 2002: Understanding Differences between the Equatorial Pacific as Simulated by Two Coupled GCMs. *J. Climate*, **15**, 449-469.

Storch, H. V., and F. W. Zwiers, 1999:*Statistical Analysis in Climate Research*. Cambridge University Press.

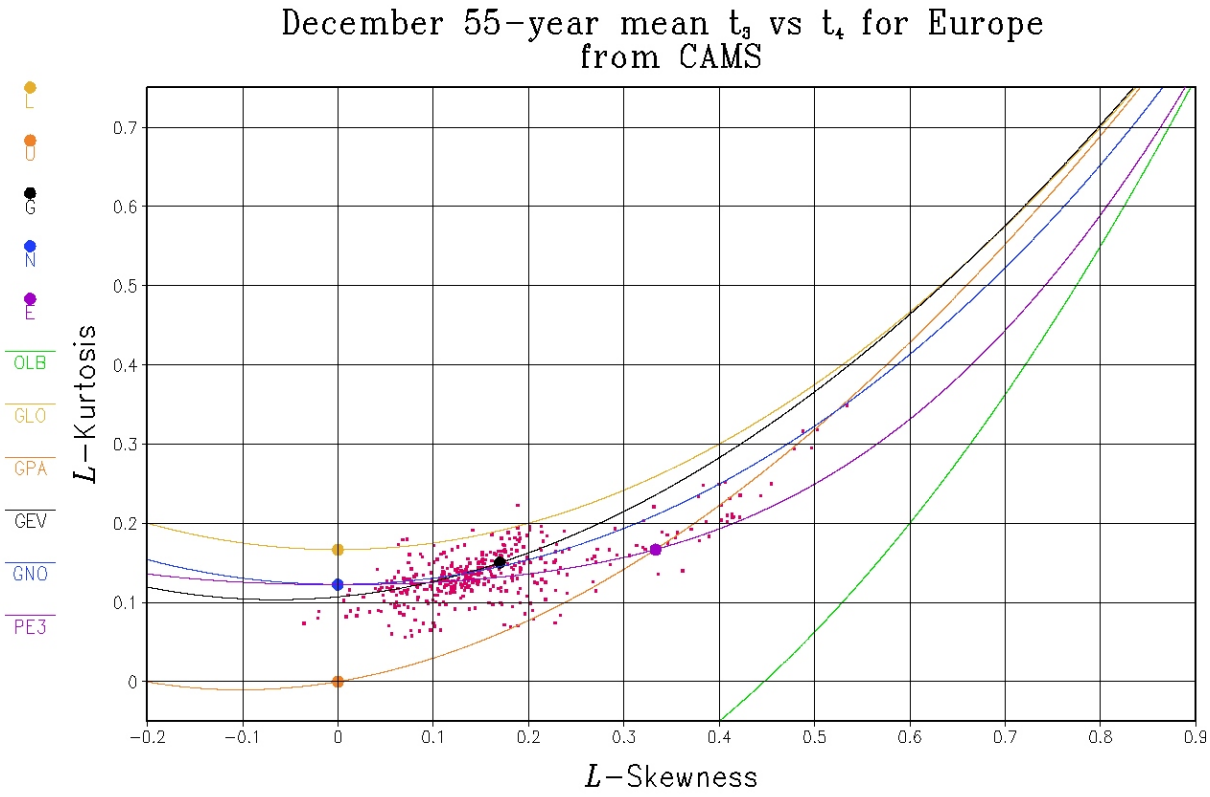
December 55-year mean t_3 vs t_4 for Europe
from CAMS
L
U
G
N
E
OLB
GLO
GPA
GEV
GNO
PE3
L-Kurtosis
L-Skewness
0
0.1
0.2
0.3
0.4
0.5
0.6
0.7
−0.2
−0.1
0
0.1
0.2
0.3
0.4
0.5
0.6
0.7
0.8
0.9

Figure 1

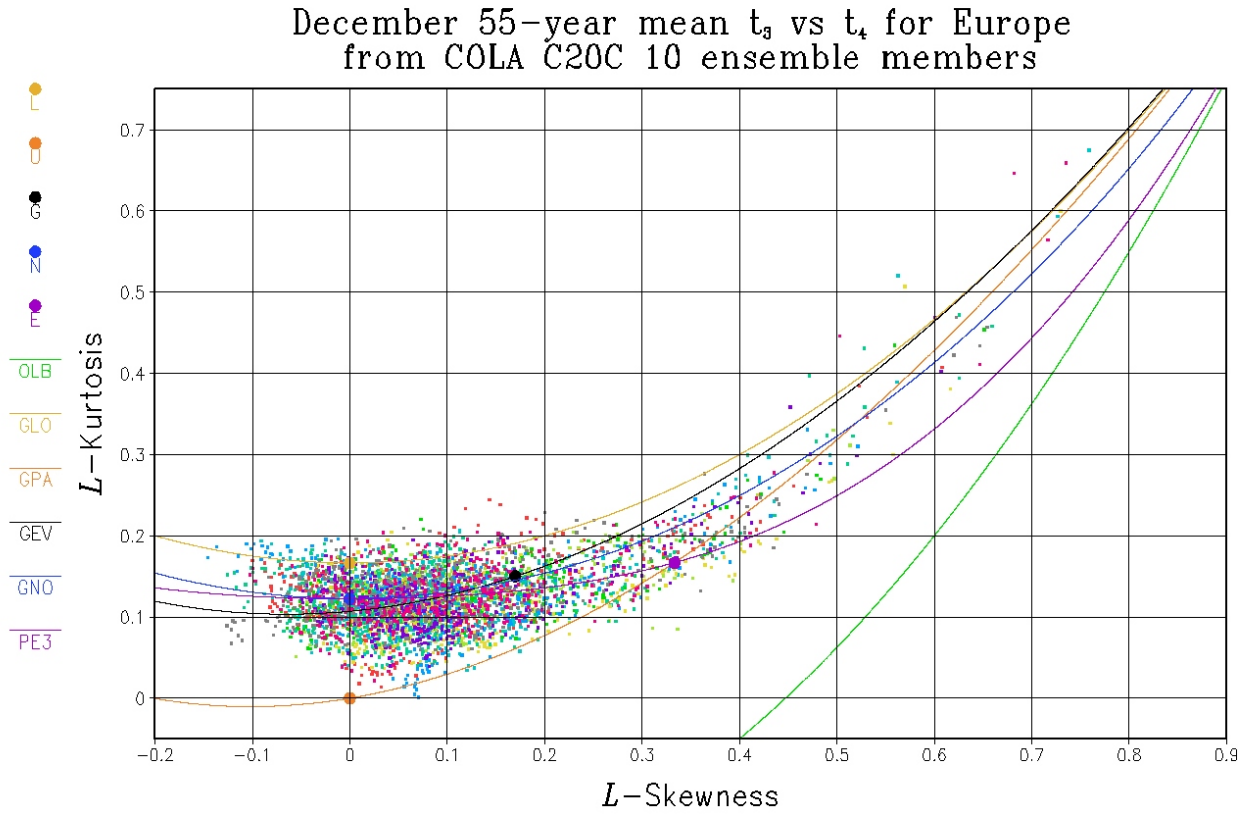
December 55-year mean t3 vs t4 for Europe
from COLA C20C 10 ensemble members
L
U
G
N
E
OLB
GLO
GPA
GEV
GNO
PE3
L-Kurtosis
L-Skewness
0
0.1
0.2
0.3
0.4
0.5
0.6
0.7
-0.2
-0.1
0
0.1
0.2
0.3
0.4
0.5
0.6
0.7
0.8
0.9

Figure 2

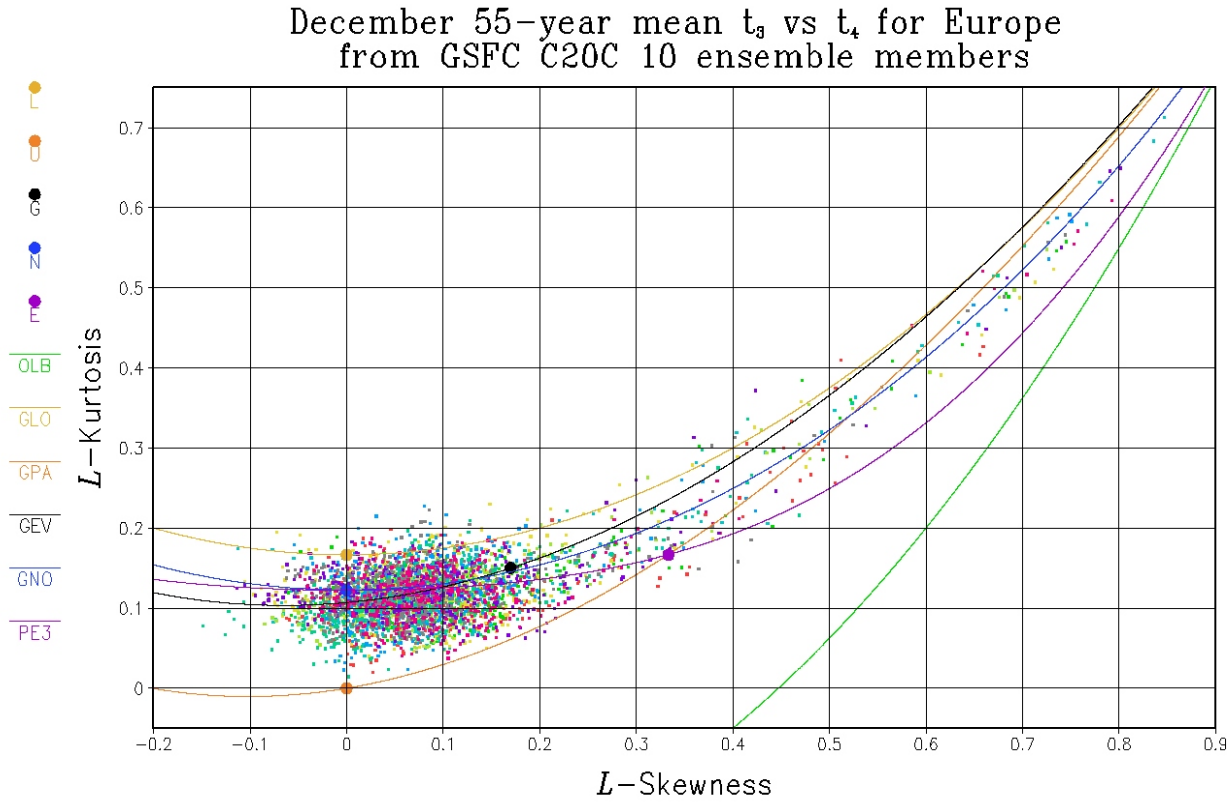
December 55-year mean t_3 vs t_4 for Europe
from GSFC C20C 10 ensemble members
L
U
G
N
E
OLB
GLO
GPA
GEV
GNO
PE3
L-Kurtosis
L-Skewness
0
0.1
0.2
0.3
0.4
0.5
0.6
0.7
−0.2
−0.1
0
0.1
0.2
0.3
0.4
0.5
0.6
0.7
0.8
0.9

Figure 3

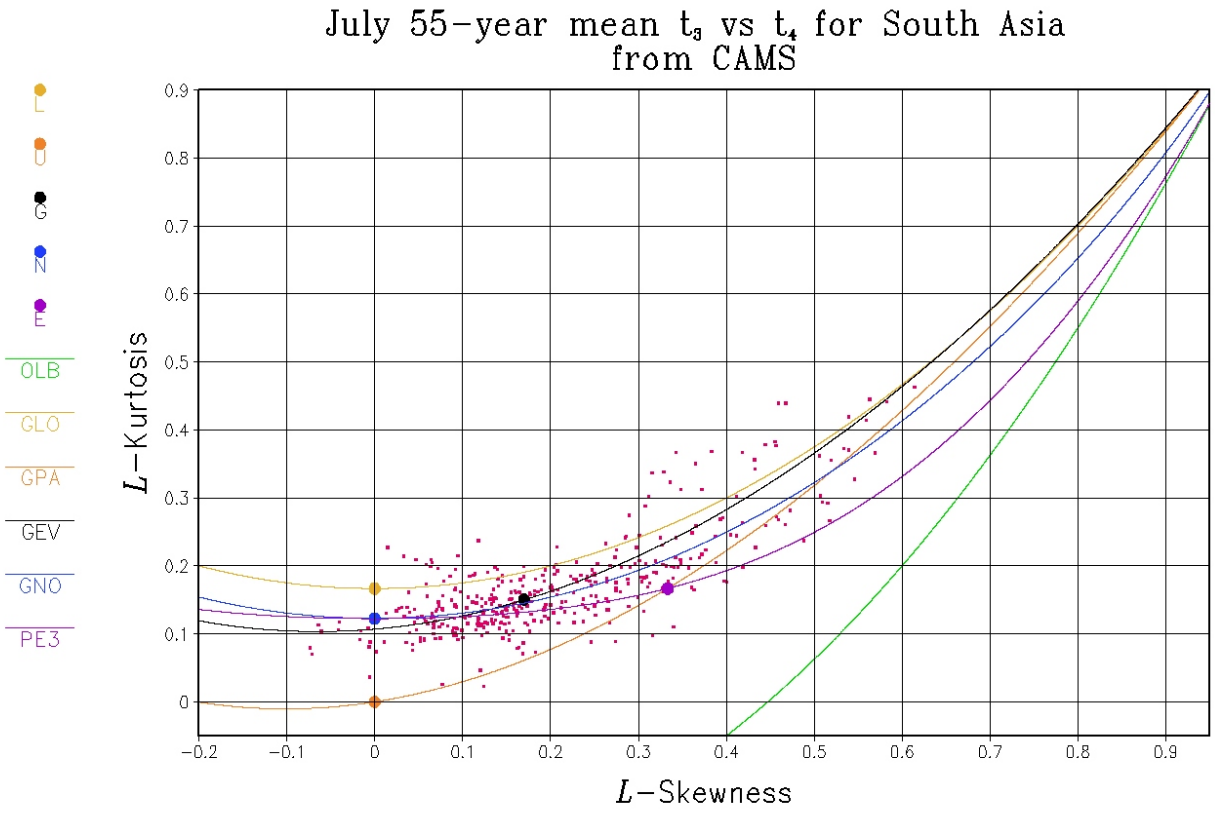
July 55-year mean t₃ vs t₄ for South Asia
from CAMS
L
U
G
N
E
OLB
GLO
GPA
GEV
GNO
PE3
L-Kurtosis
L-Skewness
0.9
0.8
0.7
0.6
0.5
0.4
0.3
0.2
0.1
0
−0.2
−0.1
0
0.1
0.2
0.3
0.4
0.5
0.6
0.7
0.8
0.9

Figure 4

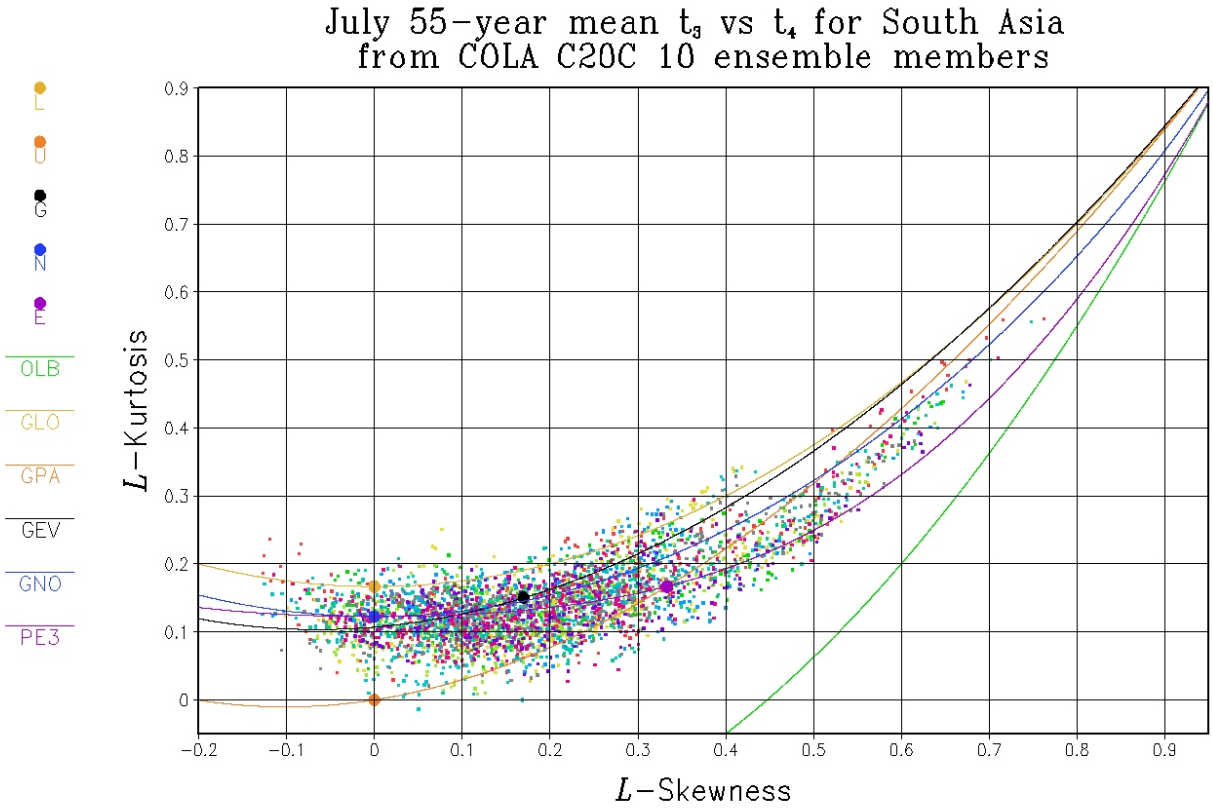
July 55-year mean t_3 vs t_4 for South Asia
from COLA C20C 10 ensemble members
L
U
G
N
E
OLB
GLO
GPA
GEV
GNO
PE3
L-Kurtosis
L-Skewness
0.9
0.8
0.7
0.6
0.5
0.4
0.3
0.2
0.1
0
−0.2
−0.1
0
0.1
0.2
0.3
0.4
0.5
0.6
0.7
0.8
0.9

Figure 5

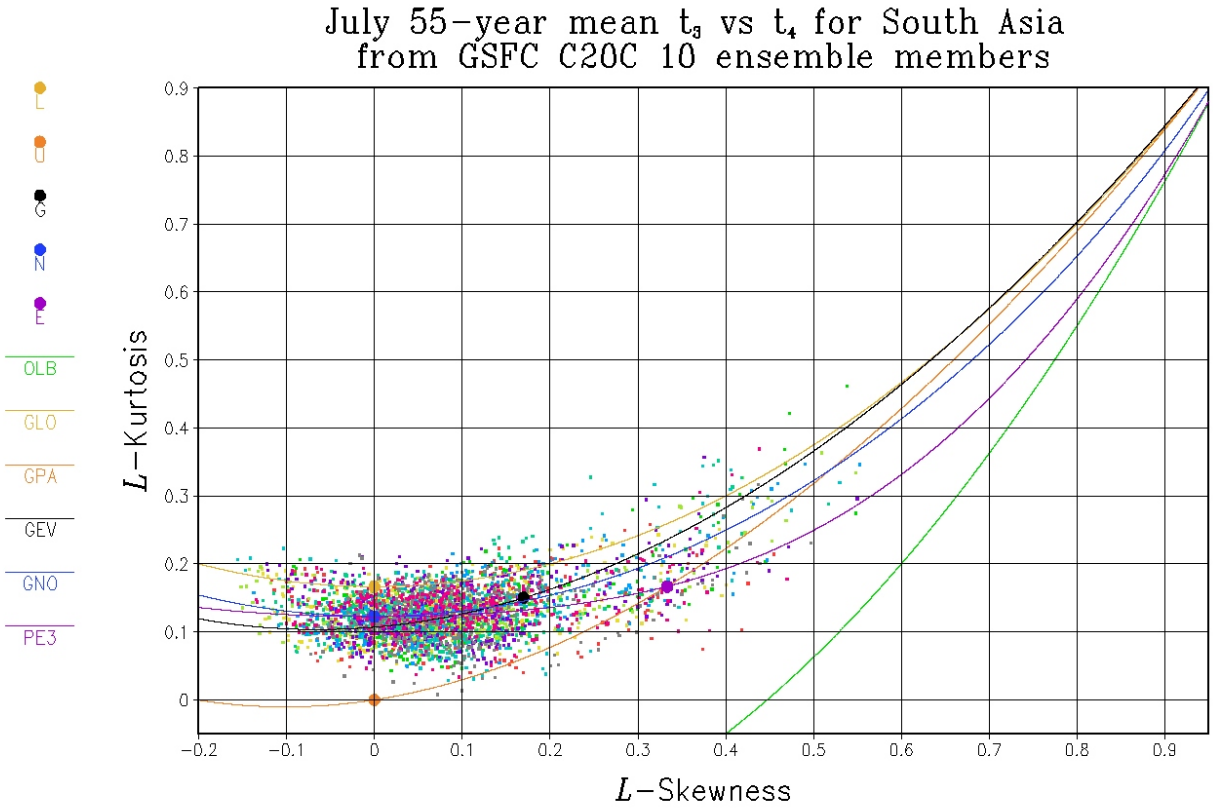
July 55-year mean t_3 vs t_4 for South Asia
from GSFC C20C 10 ensemble members
L
U
G
N
E
OLB
GLO
GPA
GEV
GNO
PE3
L-Kurtosis
L-Skewness
0.9
0.8
0.7
0.6
0.5
0.4
0.3
0.2
0.1
0
−0.2
−0.1
0
0.1
0.2
0.3
0.4
0.5
0.6
0.7
0.8
0.9

Figure 6